Finite-band solitons in the Kronig-Penney model with the cubic-quintic nonlinearity

Ilya M. Merhasin,[1,*] Boris V. Gisin,[1,2,†] Rodislav Driben,[1,‡] and Boris A. Malomed[1,§]
[1]*Department of Interdisciplinary Studies, Faculty of Engineering, Tel Aviv University, Tel Aviv 69978, Israel*
[2]*Department of Electrical Engineering - Physical Electronics, Faculty of Engineering, Tel Aviv University, Tel Aviv 69978, Israel*
(Received 19 July 2004; published 24 January 2005)

We present a model combining a periodic array of rectangular potential wells [the Kronig-Penney (KP) potential] and the cubic-quintic (CQ) nonlinearity. A plethora of soliton states is found in the system: fundamental single-humped solitons, symmetric and antisymmetric double-humped ones, three-peak solitons with and without the phase shift π between the peaks, etc. If the potential profile is shallow, the solitons belong to the semi-infinite gap beneath the band structure of the linear KP model, while finite gaps between the Bloch bands remain empty. However, in contrast with the situation known in the model combining a periodic potential and the self-focusing Kerr nonlinearity, the solitons fill only a finite zone near the top of the semi-infinite gap, which is a consequence of the saturable character of the CQ nonlinearity. If the potential structure is much deeper, then fundamental and double (both symmetric and antisymmetric) solitons with a flat-top shape are found in the finite gaps. Computation of stability eigenvalues for small perturbations and direct simulations show that all the solitons are stable. In the shallow KP potential, the soliton characteristics, in the form of the integral power Q (or width w) versus the propagation constant k, reveal strong bistability, with two and, sometimes, four different solutions found for a given k (the bistability disappears with the increase of the depth of the potential). Disobeying the Vakhitov-Kolokolov criterion, the solution branches with *both* $dQ/dk>0$ and $dQ/dk<0$ are *stable*. The curve $Q(k)$ corresponding to each particular type of the solution (with a given number of local peaks and definite symmetry) ends at a finite maximum value of Q (breathers are found past the end points). The increase of the integral power gives rise to additional peaks in the soliton's shape, each corresponding to a subpulse trapped in a local channel of the KP structure (a *beam-splitting* property). It is plausible that these features are shared by other models combining saturable nonlinearity and a periodic substrate.

DOI: 10.1103/PhysRevE.71.016613 PACS number(s): 42.65.Tg, 42.70.Nq, 05.45.Yv, 03.75.Lm

I. INTRODUCTION

Spatial solitons in multichannel optical systems are a subject of interest for fundamental studies and offer potential applications to photonics. The prototypical model of this type is based on the one-dimensional (1D) nonlinear Schrödinger (NLS) equation, which governs the evolution of the local amplitude $\Psi(z,x)$ of the electromagnetic wave along the axis z in a planar nonlinear optical waveguide with the local refractive index periodically modulated along the transverse coordinate x. In normalized units (see, e.g., Ref. [1]), this equation is

$$i\frac{\partial\Psi}{\partial z}+\frac{\partial^2\Psi}{\partial x^2}+n_0(x)\Psi+\delta n(|\Psi|^2)\Psi=0, \tag{1}$$

where $n_0(x)$ is proportional to a local change of the linear refractive index and $\delta n(|\Psi|^2)$ is the nonlinear correction to it; $\delta n(|\Psi|^2)=n_2|\Psi|^2$, with $n_2>0$, in the case of the ordinary Kerr nonlinearity. Solitons in Eq. (1) with the Kerr nonlinear term and sinusoidal transverse modulation with a period L, $n_0(x)=\epsilon\sin(2\pi x/L)$, were studied in Ref. [1]. In that work it was shown, in a numerical form and by means of a variational approximation, that the model supports a family of single-humped (SH) solitons, pinned at a center of a local potential well (waveguiding channel). The integral power (norm) of the SH soliton

$$Q\equiv\int_{-\infty}^{+\infty}|\Psi(x)|^2dx, \tag{2}$$

which is a dynamical invariant of Eq. (1), may take any value, $0<Q<\infty$, the entire family being stable. Symmetric double-humped (SDH) solitons, which may be regarded as bound states of two in-phase SH solitons, were also found in Ref. [1], with a conclusion that, for a fixed distance L between adjacent waveguiding cores, the symmetric solitons with two distinct peaks exist up to a certain minimum value of the propagation constant k (its definition is given below), and an attempt to create an SDH soliton with a smaller value of k leads to a merger of the double-humped structure into a single-humped one. Besides that, it was demonstrated that a "hot spot" (i.e., a strong localized attraction center) modeled by an extra term $\sim\delta(x-x_0)\delta(z-z_0)\Psi$ in Eq. (1), with x_0 fixed at the midpoint between two adjacent guiding channels, is able to pull the SH soliton from one channel to the other, which may be used for applications to all-optical switching.

Later, exactly the same model, based on Eq. (1) with the Kerr nonlinearity and $n_0(x)=\epsilon\sin(2\pi x/L)$, z being replaced by time t, attracted attention as a model of a strongly elon-

*Email address: merkhasi@post.tau.ac.il
†Email address: gisin@eng.tau.ac.il
‡Email address: radik@eng.tau.ac.il
§Email address: malomed@eng.tau.ac.il

gated (effectively 1D) Bose-Einstein condensate (BEC) with attractive interactions between atoms, loaded in an optical-lattice (OL) potential [2]. In particular, if the OL is strong enough, the periodic potential splits the BEC into an array of weakly coupled droplets, which suggests the use of a quasi-discrete approximation for the investigation of the corresponding solitons [3] (this approximation has become a topic of intensive studies in the context of BECs [4]).

It is relevant to mention that a multidimensional generalization of Eq. (1), with $\partial^2/\partial x^2$ replaced by the two- or three-dimensional Laplacian, and the periodic potential made multidimensional, is also a relevant model for the description of the BEC in OLs, this multidimensional model, too, supporting stable solitons [5]. The 2D version of the model applies to nonlinear photonic crystals as well (although in the latter case, the nonlinearity coefficient may also be subject to the transverse modulation), where stable spatial solitons have recently been predicted [6]. Actually, transverse modulation of the refractive index in optics can be created not only through a small periodic variation of the optical density, but also—in photorefractive media—in a *virtual form*, by means of a system of strong transverse laser beams illuminating the sample [7].

New dynamical features of solitons and possibilities for applications arise in media with nonlinearities different from the cubic one. The simplest non-Kerr nonlinearity in optical media is based on a combination of the self-focusing cubic and self-defocusing quintic terms. Observation of the cubic-quintic (CQ) optical nonlinearity was reported in the PTS crystal [8], chalcogenide glasses [9], and certain organic materials [10] (a caveat is that it may come along with strong nonlinear absorption [11]; however, for short propagation distances, relevant to experiments with spatial solitons [13], the loss may be insignificant, as analyzed in detail in Ref. [12]).

Models were also elaborated that applied the CQ nonlinearity to BECs, where the self-repulsive quintic term intends to account for three-particle collisions competing against binary collisions with the negative scattering length (which corresponds to the attractive interactions) [14]. However, in this case the nonlinear-loss term, which takes into regard a possibility that the triple collisions kick out atoms from the BEC into an incoherent component of the gas, must also be taken into regard, and, as the BEC evolves in time rather than in z, an accumulating effect of the nonlinear loss is expected to be more damaging [15].

The NLS equation (1) with the CQ nonlinearity can be cast, after imposing appropriate normalization, in the following form:

$$i\frac{\partial \Psi}{\partial z} + \frac{\partial^2 \Psi}{\partial x^2} + W(x)\Psi + 2|\Psi|^2\Psi - |\Psi|^4\Psi = 0. \tag{3}$$

Indeed, the ratio between the nonlinear coefficients, as set in Eq. (3), is achieved through a rescaling on the wave field, and the coefficients in front of the terms with the derivatives are normalized through a rescaling of z and x, while the expression for the effective potential (alias the modulated part of the refractive index), $W(x)$, which is proportional to $n_0(x)$ from Eq. (1), remains arbitrary. Solitons are sought for in the usual form, $\Psi(x,z)=\exp(ikz)R(x)$, where k is the propagation constant, and $R(x)$ obeys the equation

$$-kR + R'' + W(x)R + 2R^3 - R^5 = 0. \tag{4}$$

In the free space, with $W(x)\equiv 0$, an exact soliton solution to Eq. (4) is well known [17],

$$R^2(x) = \frac{2k}{1+\sqrt{1-4k/3}\cosh(2\sqrt{k}x)}, \tag{5}$$

where the propagation constant takes values in an interval bounded by a threshold, $0<k<k_{\rm thr}\equiv 3/4$. The integral power (2) of the exact soliton solution (5) is

$$Q_0(k) = \frac{\sqrt{3}}{2}\ln\left(\frac{\sqrt{3}+2\sqrt{k}}{\sqrt{3}-2\sqrt{k}}\right). \tag{6}$$

Recently, solitons in the CQ model, combined with the modulation of the refractive index corresponding to a single waveguide (channel), were studied in detail in Ref. [16]. The guiding channel of a width D and depth $U>0$ corresponds to

$$W(x) = \begin{cases} 0, & |x| > D/2 \\ U, & |x| < D/2 \end{cases}. \tag{7}$$

A drastic difference between the CQ solitons in the free space, which are given by Eq. (4), and those trapped in the channel is a *bistability* of the soliton family: in the region of $\frac{3}{4}<k<k_{\rm max}$ above the aforementioned threshold, where the free-space solitons do not exist ($k_{\rm max}$ depends on the channel's depth, so that $k_{\rm max}\approx U+\frac{3}{4}$ for U sufficiently large), the channel supports two different soliton solutions, "tall" and "low" ones (called in this way due to difference in their amplitudes), which pertain to the same value of k. Simultaneously, the tall solitons are broader and the low ones are narrower. On the other hand, exactly one soliton exists (as in the free-space CQ model) in the region of $0<k<\frac{3}{4}$.

No soliton bistability occurs in the same guiding channel with the usual Kerr (cubic-only) nonlinearity. In fact, in this case the soliton solutions are in one-to-one correspondence with modal eigenfunctions of the corresponding linear channel waveguide and may be classified according to the number of zeros in the solution (so that a given number of zeros defines a single soliton) [18].

An important issue is stability of the soliton solutions. In the free-space models, it frequently happens that one of the two coexisting soliton branches is stable, while the other one is not. This is suggested by the known Vakhitov-Kolokolov (VK) criterion, which, for those models where its validity can be proven, gives a necessary stability condition for a solution branch characterized by the dependence $Q(k)$ [19]: $dQ/dk>0$. Coexisting branches feature opposite signs of this derivative (see below). Nevertheless, systematic stability tests based on direct simulations have demonstrated that *both* soliton branches in the CQ-nonlinear channel waveguide are *stable*, i.e., the VK criterion does not apply to that model. Such a bistability is, obviously, promising for applications to all-optical switching. Curiously, in this model the VK criterion fails in a way *opposite* to how this is known to occur in

other cases, when some solitons, which are predicted by the criterion to be stable, turn out to be unstable (against perturbation modes corresponding to complex eigenvalues, for which the VK criterion is irrelevant). An example of that is provided by the family of gap solitons in the standard model of a fiber Bragg grating [20].

The objective of this work is to find various species of solitons in the CQ model combined with a periodic array of waveguides, corresponding to a periodic function $n_0(x)$ in Eqs. (1) and (4). In order to introduce a model that is closer to optical multichannel systems, we assume the modulation of $n_0(x)$ in the form of a periodic (with a period L) array of waveguiding cores of the width D, separated by buffer layers of the width $L-D$ [cf. the expression (7) for the channel waveguide],

$$W(x) = \begin{cases} 0, & D + Ln < x < L(1+n) - D \\ U, & Ln < x < D + Ln \end{cases}, \quad n = 0,1,2,\cdots. \tag{8}$$

Note that the linear Schrödinger equation with the periodic potential in the form of $U(x) = -W(x)$, where $W(x)$ is taken in the form of Eq. (8), constitutes the well-known Kronig-Penney (KP) model, which admits calculation of the corresponding band structure in an analytical form [21] (solitons in a model combining the KP potential and the usual cubic nonlinearity were very recently considered in Ref. [22]).

Once the underlying CQ NLS equation was fixed in the form of Eq. (1), the parameters U, D, and L of the KP potential (8) are irreducible. To them, the integral power (2) must be added as an intrinsic parameter of the soliton families.

In this work, we find several species of stable solitons in the CQ-nonlinear KP model. First of all, in the case of a relatively weak KP potential, we find, together with two coexisting *stable* branches of the fundamental (SH) solitons (similar to those found in Ref. [16] in the single-channel model), various types of stable higher-order solitons, including symmetric and antisymmetric double-humped (SDH and ASDH) ones, two kinds of three-humped (TH) solitons, with the phase difference zero or π between the central and side peaks, and so on. Similar to the SH solutions, each family of the multi-humped solitons features the bistability. A principal difference from the CQ single-channel model in which the integral power Q of the SH soliton takes all the values from 0 to ∞ is that, in the KP model, the SH soliton exists up to a finite maximum value $Q_{\max}^{(\mathrm{SH})}$, above which only multihumped solitons can be found (an attempt to increase Q by a small increment above the maximum value leads to appearance of a persistent breather instead of the stationary soliton). In fact, the CQ-nonlinear KP model features a *beam-splitting* property, which may be of obvious interest to applications: solitons of any type, with a given number of the peaks, are stable, but they exist in a finite range of Q; the increase of the integral power results in consecutive appearance of additional peaks, which correspond to subpulses trapped in local channels of the periodic structure. Quite plausibly, the latter feature is common to a general class of models with *saturable nonlinearity*, of which the CQ one is a simplest representative. With the transition to a strong KP potential, the bistability disappears.

Another distinctive feature of the CQ model with the periodic substrate is the band structure of the soliton solutions. We will demonstrate that, as well as in the model combining the self-focusing Kerr nonlinearity and a periodic potential, the solitons tend to belong to a semi-infinite gap under the bottom of the Bloch band structure corresponding to the given periodic potential in the linear model, while finite gaps between the Bloch bands remain empty (nevertheless, solitons are also found in the finite gaps, if the KP potential is strong enough). However, in contrast to the situation in the Kerr model, the fundamental-soliton band is *finite* itself, being localized near the top of the semi-infinite gap.

Another step ahead made in this paper in comparison with the study of solitons in the single-channel CQ model considered in Ref. [16] is that the solitons' stability was investigated there only in direct simulations. In this work, we explore the stability by means of both computation of the corresponding eigenvalues from the linearized version of Eq. (1), and in direct simulations. As a result, we conclude that all the solitons (at least, with up to five humps) are stable. Importantly, in all the cases, the coexisting branches of the soliton solutions (two or, sometimes, four), with both $dQ/dk > 0$ and $dQ/dk < 0$, are found to be completely stable; note that the branch of the latter kind are stable *contrary* to the prediction of the VK criterion.

The paper is organized as follows. In Sec. II, we present results for the fundamental (SH) solitons, including their stability and location in the k space relative to the band structure of the KP potential, in the case when the potential is relatively weak, and solitons exist solely in the semi-infinite band. For the same case, results for the double-humped solitons, of both SDH and ASDH types, are summarized in Sec. III, and, for the TH solitons together with some higher-order ones, in Section IV. In Sec. V, we briefly consider the case of a strong potential, when the bistability does not take place, and stable fundamental and double-humped solitons (which are very different from those existing in the semi-infinite gap in the case of the weak potential) are found in finite gaps of the KP band structure. The paper is concluded by Sec. VI.

II. SINGLE-HUMPED SOLITONS

In Ref. [16], the CQ solitons trapped in the channel waveguide (7) were found both in a numerical form and by means of the variational approximation. In this paper, we focus on the numerical investigation, as the KP potential (8) makes variational expressions rather ponderous. As concerns analytical considerations, an exact result can be derived by integration of Eq. (4) inside each segment with $W(x) = \mathrm{const}$ and by matching the solutions at junctions between the segments, in essentially the same way as it was done for the single-channel CQ model in Ref. [16]. Assuming solitons with a single maximum, it is possible to demonstrate that the soliton's amplitude $R_{\max}$ [the maximum value of the field $R(x)$] belongs to the interval

$$\sqrt{3} - \sqrt{3 - 4(k-U)} < 2R_{\max}^2/\sqrt{3} < \sqrt{3} + \sqrt{3 - 4(k-U)} \tag{9}$$

(under certain conditions, this inequality applies to multipeaked solutions too). An obvious consequence of this in-

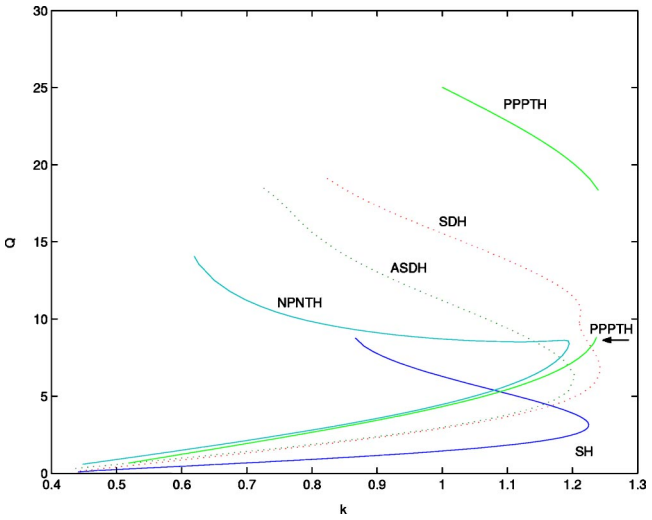

FIG. 1. (Color online) The integral power (2), Q, for the solitons of diverse types vs the propagation constant k, in the CQ nonlinear model with the periodic Kronig-Penney potential. The depth and width of the potential wells are $U=0.7$ and $D=3$, and the thickness of the buffer layer between the wells is $L-D=3$. The labels SH, SDH, and ASDH pertain, respectively, to the single-humped, symmetric double-humped, and antisymmetric double-humped solitons. Furthermore, the labels PPPTH and NPNTH mark the families of three-humped solitons of the $(+++)$ and $(-+-)$ (in the gap between the top and bottom segments of the PPPTH branch, the numerical code could not converge to a solution). Each curve ends at the maximum value of Q beyond which the corresponding soliton family does not exist, see the text.

equality is an upper limit on the propagation constant,

$$k_{\max} < U + \tfrac{3}{4} \tag{10}$$

[in the case of $U=0$, it goes over into the condition $k<\frac{3}{4}$ for the exact free-space soliton (5)]. It is relevant to note that, in the case of the Kerr (cubic-only) nonlinearity, one obtains a less restrictive and less definite inequality instead of Eq. (9), $k<U+[R_{\max}(k)]^2$ [18]. In fact, the latter result implies that the values of k available to the fundamental solitons in the Kerr model are not limited (see also Ref. [22]), while Eq. (10) shows that in the CQ model, k is definitely bounded from above. This fact will have important consequences concerning the soliton bands in the model (see below).

As well as in the case of the one-channel model, the numerical solution of the stationary equation (4) with the KP substrate yields a single fundamental (SH) solution for a given k, if k is smaller than a certain threshold value $k_{\rm thr}$; in the region of $k_{\rm thr}<k<k_{\max}$, there are two coexisting SH solitons and no solution is found for $k>k_{\max}$ [see also Eq. (10)]. In Fig. 1, this situation is illustrated by a generic example of the curve $Q(k)$ (the figure includes similar characteristics for higher-order solitons, see details below).

We stress that, at values of Q larger than $Q_{\max}^{(\rm SH)}\approx 9$, at which the fundamental-soliton curve ends in Fig. 1, SH solitons do not exist (or, at least, the numerical algorithm could not converge to such a soliton). The nonexistence of the SH solitons at large Q is a specific feature of the present model,

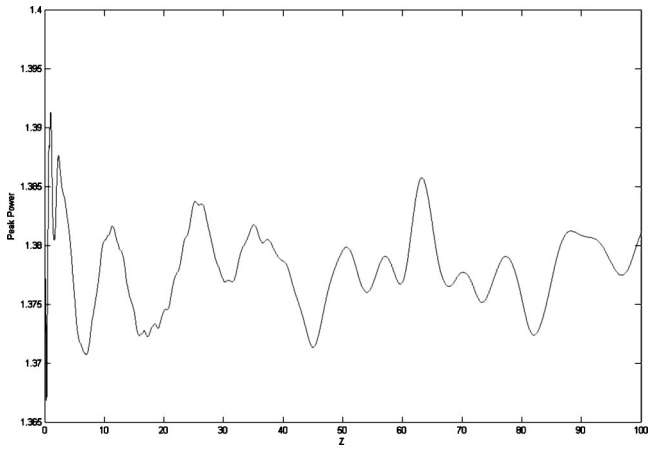

FIG. 2. An example of the single-humped breather, obtained from the single-humped (SH) soliton corresponding to the end point of the SH branch in Fig. 1, by stretching it with the factor $1+\varepsilon=1.1$. Shown is the peak power of the resulting solution, $|\Psi(x=0)|^2$ vs z. Note a very small amplitude of the irregular oscillations around a mean value of the peak power.

which can be understood as follows. In the model with the CQ nonlinearity, the amplitude of the solitons is limited due to the presence of the self-defocusing term, which is obvious from the exact solution for the free-space soliton (5), where $R(x)\leqslant\sqrt{3/2}$. Therefore, the increase of the soliton's integral power (norm) can only go via the increase of its width; in particular, the width of the exact soliton (5) diverges $\sim\ln[1/(k_{\rm thr}-k)]$ as one approaches the threshold value $k_{\rm thr}=\frac{3}{4}$ [this is also obvious from the expression (6) for the soliton's norm]. The indefinite increase of the soliton's width is possible, indeed, in the free space, as well as in the case when the soliton is pinned in one channel [16]. However, the expansion of the soliton on top of a periodic substrate inevitably leads to formation of new peaks (humps), as will be shown in detail below. On the other hand, in the model with the cubic-only nonlinearity, very large Q implies that the soliton's amplitude is very large, $\sim Q$, and its width is very small, $\sim 1/Q$, therefore, an SH soliton with an indefinitely large norm can exist in the periodic potential [1].

We also tried to check what happens in direct simulations (rather than when searching for stationary solutions) as a result of an attempt to create an SH soliton with the integral power exceeding $Q_{\max}^{(\rm SH)}$. To this end, the soliton corresponding to $Q=Q_{\max}^{(\rm SH)}$ was stretched, replacing $R(x)$ by $\widetilde{R}(x)\equiv R[(1+\varepsilon)x]$ with $\varepsilon>0$, and the thus-stretched pulse was then used as the initial configuration for direct simulations of Eq. (3). With ε relatively small (for instance $\varepsilon=0.1$), the simulations generate a nearly stationary soliton with very weak (small-amplitude) and irregular, but persistent, intrinsic vibrations (a *single-humped breather*), see an example in Fig. 2. For larger ε (for example, $\varepsilon=0.25$), the result is different: in accordance with the explanation given above, new side peaks are formed in the wings of the soliton, pulling into themselves a bigger part of the total power; then, a large share of the power returns to the central peak, and the power-exchange cycle repeats itself quasiperiodically, as shown in Fig. 3. We stress that, although the side peaks may be small

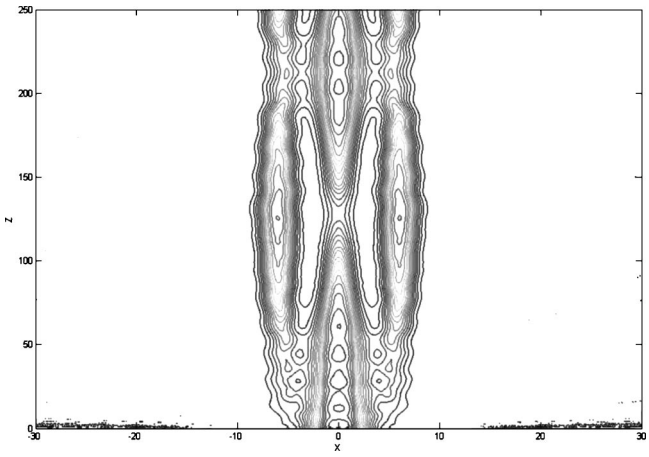

FIG. 3. Contour plots show a three-humped breather obtained from the SH soliton corresponding to the end point of the SH branch in Fig. 1, by stretching it with the factor $1+\varepsilon=1.25$.

at some stage of the oscillations, they never disappear; hence, this object may be called a *three-humped breather*. In both cases shown in Figs. 2 and 3, examination of the numerical data demonstrates that the breather does not suffer any tangible radiation loss.

Typical examples of the fundamental solitons in the bistability range, where Fig. 1 predicts two SH solitons with different amplitude and width for the same k, are displayed in Fig. 4. We note that because the soliton's field decays, at $|x|\to\infty$, as $\exp(-\sqrt{k}|x|)$, and the maximum value of k attainable by the soliton trapped in the potential structure is essentially larger than $k_{\rm thr}=\frac{3}{4}$ in the free space, the trapped soliton may have sharper edges than the free one, which is a clear advantage for the multichannel systems employing spatial solitons. The fact that the trapped CQ solitons have sharper edges than their counterparts in the free space is, indeed,

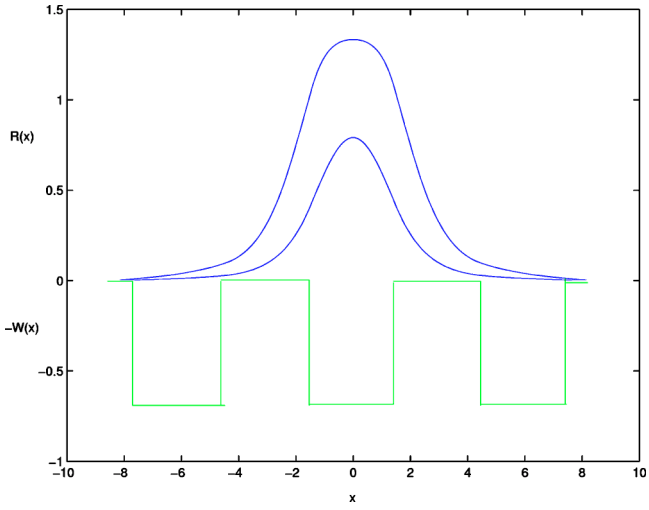

FIG. 4. (Color online) Two typical examples of the fundamental soliton, for the same parameters as in Fig. 1. Both solitons pertain to the propagation constant $k=1$ (the soliton with the larger and smaller amplitude pertains, respectively, to the upper and lower branch in Fig. 1). The underlying Kronig-Penney potential $-W(x)$ is shown in the lower part of the figure.

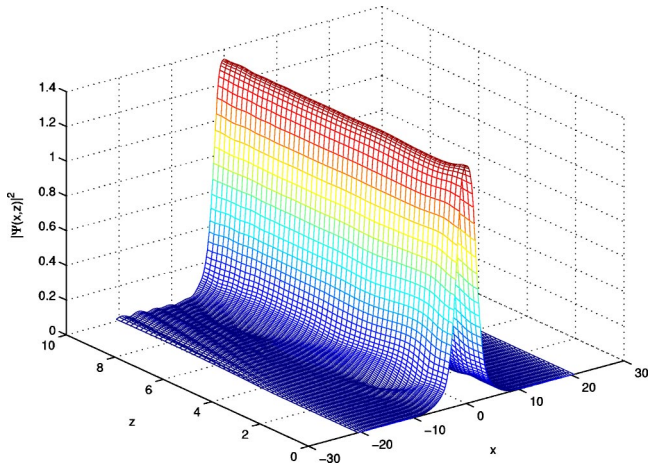

FIG. 5. (Color online) A typical example of stable evolution of the fundamental (single-humped) soliton (its unperturbed form is the upper one in Fig. 4) with an initial perturbation whose amplitude is 3% of the soliton's amplitude.

corroborated by a detailed consideration of the solitons' shapes.

Stability of the SH solitons was checked by means of the numerical computation of eigen-values of small perturbations, linearizing Eq. (1) around the stationary soliton solutions. The result is simple: all the fundamental solitons are stable. The spectrum of the eigenfrequencies contains one zero value, all the other ones being real (an example of the spectrum will be displayed below for the case of SDH solitons, see Fig. 9). The stability was also checked directly, in simulations of a soliton that was randomly perturbed at the initial point, $z=0$. An example that illustrates the stability of all the fundamental solitons is displayed in Fig. 5.

It seems plausible that an input beam whose profile is far from the exact soliton will self-trap not into a static soliton, but rather into a breather, similar to what is shown in Figs. 2 and 3 and was shown in detail in Ref. [16] for the CQ model with the single-channel potential (7). More detailed consideration of this issue is beyond the scope of this work.

It is obvious from Fig. 1 that the upper branch of the SH-soliton family *does not* satisfy the VK stability criterion, $dQ/dk>0$ [19]. Nevertheless, both the stability eigenvalues and direct simulations clearly demonstrate that the entire upper branch is stable (as well as its lower counterpart). In particular, the stable soliton displayed in Fig. 5 belongs to the upper branch. Thus, the VK criterion fails in the case of the model combining the CQ nonlinearity and the potential. (The same was already concluded, for the case of the single-channel potential, in Ref. [16]; however, in that work the stability was not verified by computation of the eigenvalues.) On the other hand, the validity of the criterion for this type of system has never been proven, to the best of our knowledge. In any case, this result demonstrates validity limits of the VK criterion.

An important issue is to identify the location of the solitons, in the k space, relative to the underlying band structure of the linear KP model. The corresponding quasiperiodic Bloch modes have the usual form, $R(x)=\exp(iqx)P(x)$, where q is a real quasimomentum (in terms of quantum me-

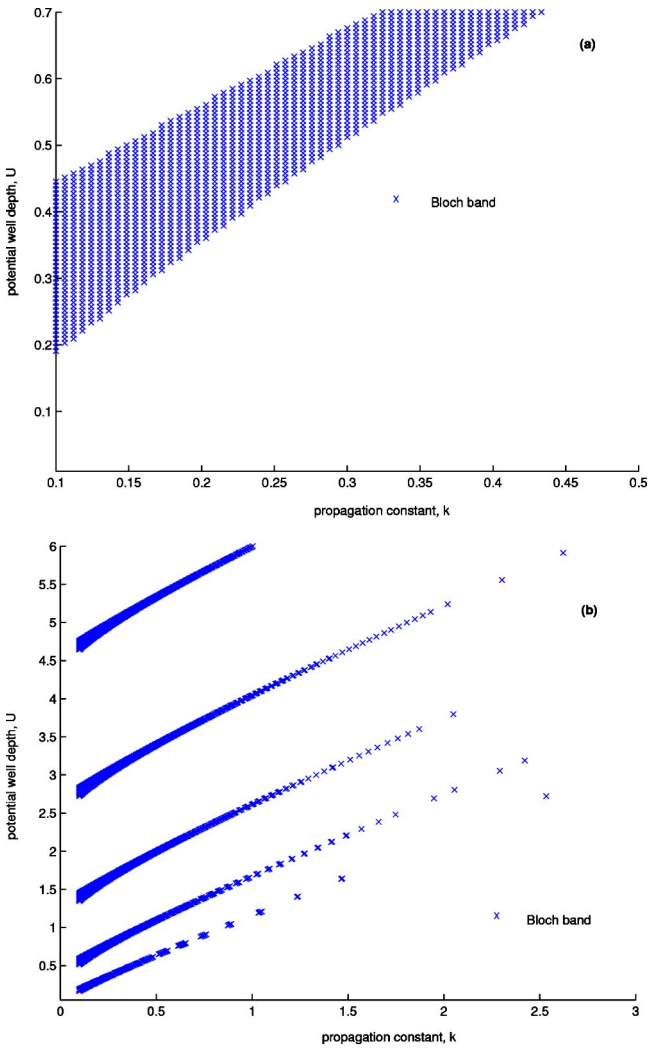

FIG. 6. Typical examples of the Bloch-band structure in the Kronig-Penney model with a weak (a) and strong (b) potential. The parameters are $U=0.7$ and $D=L-D=3$ in (a) and $U=6$ and $D=L-D=6$ in (b). The entire region of $k<0$ is a semi-infinite band.

chanics), and $P(x)$ is a periodic function with the period L. As is known [21], the band structure of the KP potential (8), $k=k(q)$, is determined by a relation

$$\frac{k-\tilde{k}}{2\sqrt{k\tilde{k}}}\sinh\left[(L-D)\sqrt{k}\right]\sin\left(D\sqrt{\tilde{k}}\right) + \cosh\left[(L-D)\sqrt{k}\right]\cos\left(D\sqrt{\tilde{k}}\right)=\cos(Lq), \quad (11)$$

where $\tilde{k}\equiv U-k$. Equation (11) gives rise to a semi-infinite band of Bloch states at $k<0$, and several finite bands at $k>0$. The bands are separated by gaps, in which solitons may (or may not) be found in a nonlinear model. Beneath the lowest finite band, a semi-infinite gap, extending to $k\to+\infty$, is located (in particular, the entire region of $k>U$ belongs to the semi-infinite band). Typical examples of the band structure in the linear KP model, with a weak and strong potential, are displayed in Fig. 6. In particular, for large values of the product Dk, it is easy to demonstrate that the bands are exponentially narrow, with the width

$$\Delta k_{\text{band}}\sim\exp\left(-D\sqrt{k}\right). \quad (12)$$

At typical values of parameters for a relatively weak KP potential, $U=0.7$ and $D=L-D=3$, to which Figs. 1 and 4 pertain, the linear KP model gives rise to a single finite Bloch band, $0.3195<k<0.4356$ [see Fig. 6(a)]. All the soliton families (SH and higher-order ones) presented in Fig. 1 are located in the semi-infinite gap precisely beneath this band (i.e., at $k>0.4356$), while the finite gap, $0<k<0.3195$, which separates the finite and semi-infinite bands, remains empty.

It is relevant to mention that, in the model with a periodic (in particular, sinusoidal) potential and self-attracting Kerr nonlinearity [1–3,23,24], the solitons completely fill the semi-infinite gap; if the sinusoidal potential is strong enough, then soliton solutions are found inside finite gaps too (the same is possible in the present model if the KP potential is stronger, see Sec. V). The situation is opposite in the model combining the sinusoidal potential and self-defocusing (anti-Kerr) cubic nonlinearity. In that case, the semi-infinite gap is (quite naturally) empty, while stable envelope solitons (with a negative effective mass [24]) are found in the finite gaps, as shown in Ref. [23]. (Very recently, such gap solitons have been created in the BEC loaded in an OL potential [25].)

A difference of the CQ model from the cubic one, which is obvious from Fig. 1 [and also from the inequality (10)], is that the solitons fill a finite top part of the semi-infinite band, while the rest of it remains empty. Thus, in the CQ model, the situation is, in a certain sense, intermediate between those in the Kerr and anti-Kerr models. In the case of a relatively weak potential, the soliton band lies beneath the bottom of the linear-KP band structure, but it has a finite width because of the saturable character of the nonlinearity in the CQ model.

III. DOUBLE-HUMPED SOLITONS

Two families of double-humped solitons are easily found in the present model, corresponding to even and odd solutions $R(x)$ of Eq. (4), i.e., SDH and ASDH solitons, respectively. The corresponding solution families are described by the curves $Q(k)$ shown in Fig. 1. As well as their SH (fundamental) counterparts, each family of the double-humped solitons also features the bistability, in the sense of having two different solutions corresponding to the same k from the respective interval, $k_{\text{thr}}<k<k_{\max}$. Moreover, the family of the SDH solitons demonstrates the coexistence of *four* different solutions, in a narrow interval of k close to $k_{\max}$ (so that it has *three* turning points, rather than one, in particular, at $D=L-D=3.4, U=0.7$ for SDH solitons). In fact, this feature can be more pronounced at other values of the parameters. As well as the $Q(k)$ characteristic for the SH solitons, the ones for the double-humped soliton, shown in Fig. 1, cannot be continued past the points at which they end, $Q=Q_{\max}^{(\text{SDH})}$, $Q=Q_{\max}^{(\text{ASDH})}$, and $Q=Q_{\max}^{(\text{TH})}$.

Typical examples of SDH and ASDH soliton pairs, pertaining to a common value of k, are presented in Fig. 7. It is

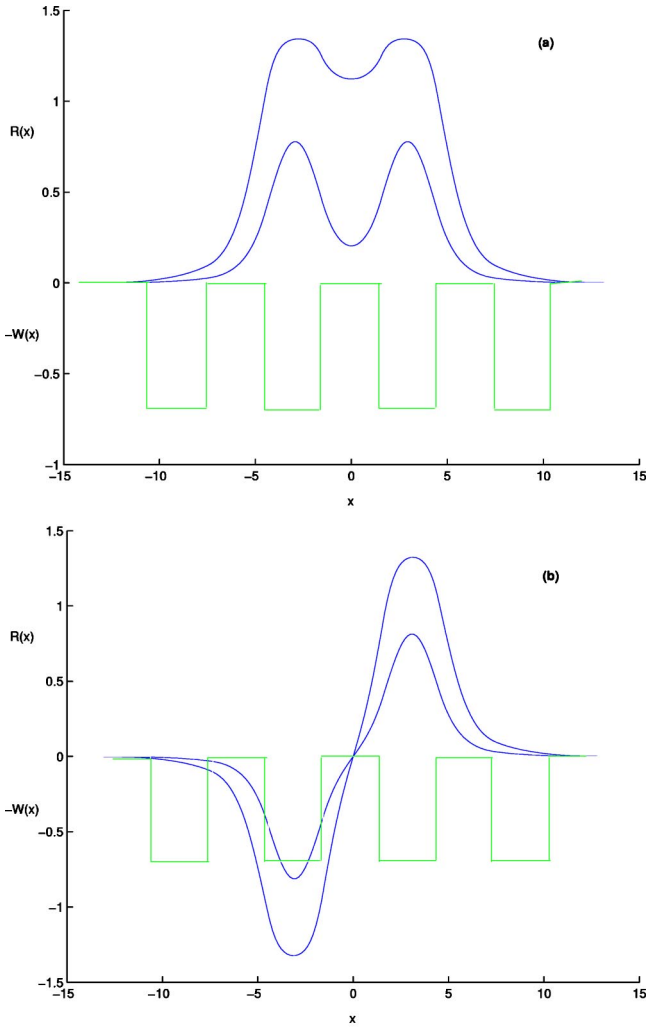

FIG. 7. (Color online) Generic examples of the symmetric (a) and antisymmetric (b) double-humped solitons belonging to the families presented in Fig. 1. In each panel, a pair of solitons found at the same value of the propagation constant, $k=1$, are displayed.

noteworthy that the $Q(k)$ curve for the SDH solitons ends at $Q_{\max}^{(\mathrm{SDH})} \approx 19.3$, which is, approximately, twice the above-mentioned end-point value, $Q_{\max}^{(\mathrm{SH})} \approx 9$, of the SH-soliton branch (pertaining to the same values of the parameters of the KP potential). For the ASDH family, the endpoint value is $Q_{\max}^{(\mathrm{ASDH})} \approx 18.7$. Together with the shapes of the SDH and ASDH solitons displayed in Fig. 7, these observations strongly suggest that the double-humped solitons may be considered as bound states of two SH solitons, with the phase shift between them 0 or π, respectively. This interpretation is strongly supported by an observation that, if the $Q(k)$ curves in Fig. 1 are redrawn so that the curve for solitons with N peaks is replaced by $Q(k)/N$ (power per peak, which actually affects the cases of $N=2$ and 3), then the bottom parts of the curves $Q(k)/N$ (those up to the turning point) are practically identical for all the families.

It may also be useful to look at the soliton families in terms of the dependence between k and the soliton's half-width w (instead of Q). To this end, we adopt the integral

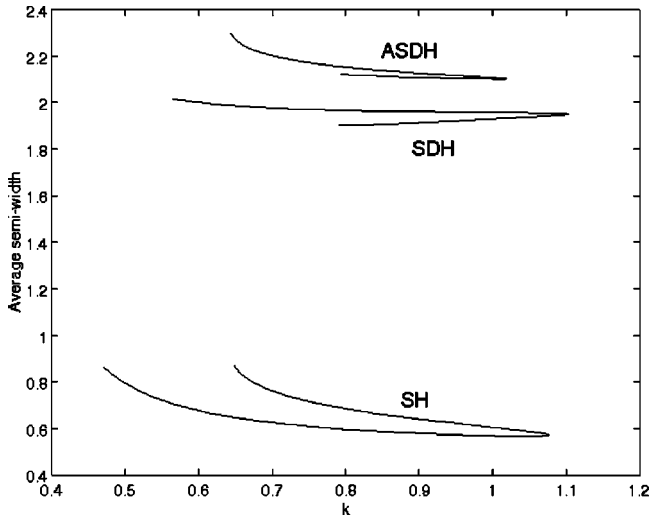

FIG. 8. Characteristics for the families of the single-humped (SH), symmetric double-humped (SDH), and antisymmetric double-humped (ASDH) solitons, in the form of the half-width w vs the propagation constant k in the model with $U=1$ and $D=L-D=2$.

definition of the half-width, as it must apply to solitons with quite different shapes:

$$w = Q^{-1} \int_0^\infty R^2(x) x dx. \tag{13}$$

Typical examples of the $w(k)$ characteristics for both the symmetric and antisymmetric double-humped solitons are displayed in Fig. 8. For comparison, the $w(k)$ characteristic for the fundamental SH soliton is also shown in the figure. As it was explained above, the soliton's amplitude in the CQ model is bounded from above; for this reason, the double-humped soliton is about three times as broad as its SH counterpart. In addition, the SDH soliton is somewhat narrower than its ASDH counterpart, as the former soliton is a "denser packed" one.

Double-humped solitons do not exist in the CQ model with the single-channel potential (7) [16], but they are known in the model with the Kerr (self-focusing cubic) nonlinearity and sinusoidal potential [1–3]. However, the double-humped solitons in the present model play a principally different role. As it was said above, in the case of the cubic nonlinearity the SH solitons exist at all the values of the integral power, up to $Q=\infty$. In the CQ model, they exist only in the region of $Q<Q_{\max}^{(\mathrm{SH})}$, as was shown above. Thus, while in the cubic model the single- and double-humped solitons exist in parallel, the *beam splitting* takes place in the CQ model. In the interval $Q_{\max}^{(\mathrm{SH})}<Q<Q_{\max}^{(\mathrm{SDH})}$, *only* the double-humped solitons are possible. [In the subinterval $Q_{\max}^{(\mathrm{SH})}<Q<Q_{\max}^{(\mathrm{ASDH})}$, both SDH and ASDH solitons are found, while in the smaller region, $Q_{\max}^{(\mathrm{ASDH})}<Q<Q_{\max}^{(\mathrm{SDH})}$, only the former type is present. For instance, in the cases shown in Fig. 1, these two intervals are, approximately, $9<Q<18.7$ and $18.7<Q<19.3$.] Of course, higher-order solitons, with more than two peaks, also exist in the same region and beyond. On the other hand, extensive numerical exploration of the pa-

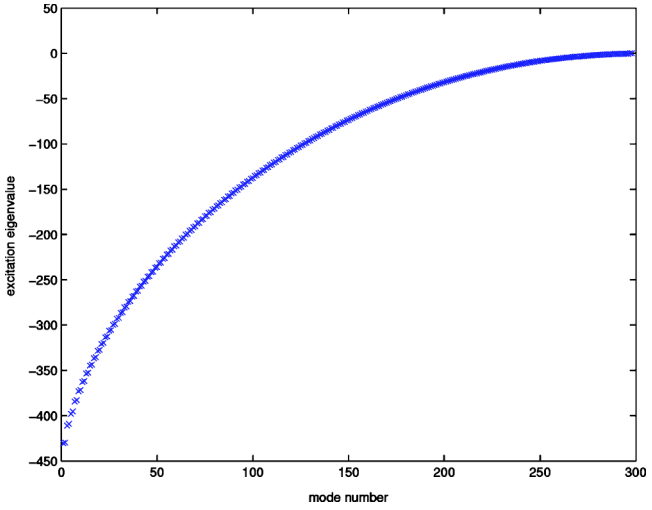

FIG. 9. The set of eigenfrequencies for small perturbations around the antisymmetric double-humped soliton, which is the taller one from Fig. 7(a).

rameter space has not turned up any example of asymmetric double-humped solitons, i.e., ones that would be neither symmetric nor antisymmetric.

The stability of the double-humped solitons was studied, as well as in the case of the SH solitons, through the computation of the eigenfrequencies of small perturbations and in direct simulations. Both methods have shown that the families of the SDH and ASDH solitons are completely stable in their entire existence regions. It is noteworthy that, in the narrow region where *four* different SDH solitons coexist (see Fig. 1), they *all* are stable.

A typical example of the full spectrum of the perturbation eigenfrequencies for an ASDH soliton is displayed in Fig. 9, and Fig. 10 shows relaxation of perturbed double-humped solitons. Note that, as well as the SH soliton family, the double-humped solitons *do not* obey the VK criterion because the branches with $dQ/dk<0$ are as stable as their counterparts with $dQ/dk>0$.

A very strong perturbation applied to a double-humped soliton can result in transition to a soliton of a different type. For example, Fig. 11 shows a strong perturbation switching the double-humped soliton into one with four peaks, which also demonstrates the existence of a plethora of higher-order solitons in the model (see also Sec. IV).

As it was mentioned above, the integral power of the double-humped solitons is bounded from above. An attempt to push the power of the SDH soliton above the maximum value results in a further step in the *beam splitting* cascade, generating extra side peaks, so that the soliton assumes a breathing (nonstationary) four-humped shape, similar to that obtained in Fig. 11 (cf. the three-humped breather in Fig. 3). Actually, in the case displayed in Fig. 11 it is observed that the attempt to make the two in-phase peaks in the SDH soliton too high induces *repulsion* between them because the self-defocusing quintic terms dominate for large values of the amplitude; as a result, a part of the power is shed off into the adjacent cells, giving rise to the extra peaks.

On the other hand, an attempt to pump too much power into the ASDH soliton leads to a different outcome: as the

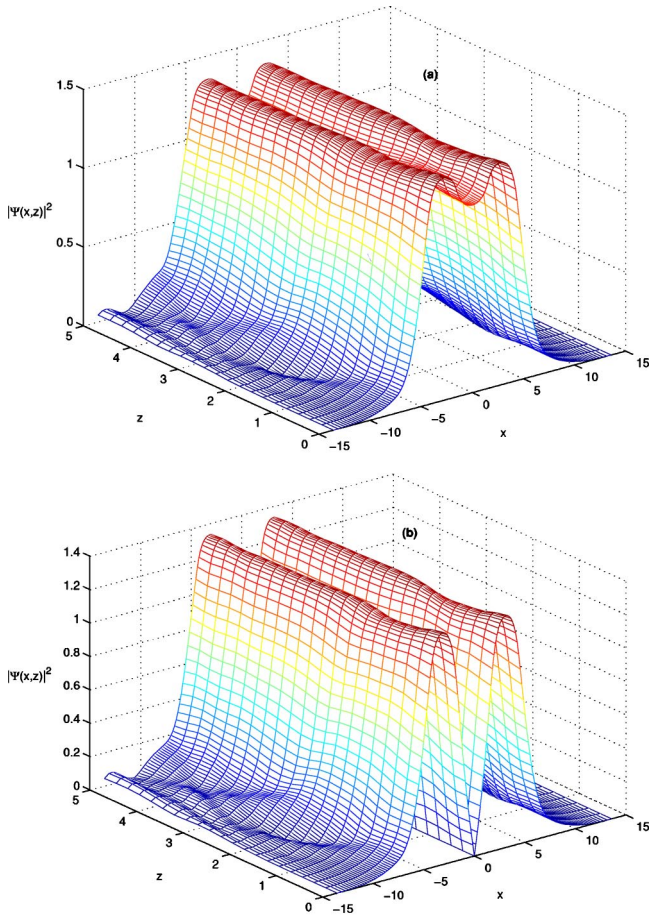

FIG. 10. (Color online) Stable relaxation of the symmetric (a) and antisymmetric (b) double-humped solitons (the same as those shown in Fig. 7) with an initial perturbation whose amplitude is 5% of the soliton's amplitude.

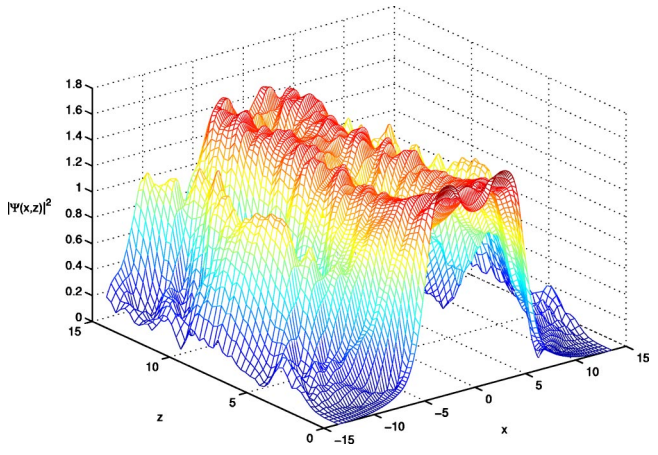

FIG. 11. (Color online) An initial perturbation whose amplitude is 20% of the soliton's amplitude switches the symmetric double-humped soliton [the same as that shown, in the unperturbed form, in Fig. 7(a)] into a higher-order nonstationary (breathing) four-humped soliton.

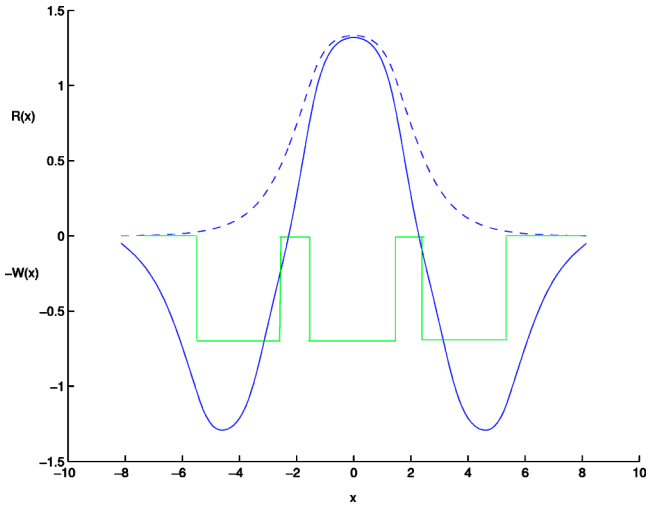

FIG. 12. (Color online) A three-humped stable soliton, found at $k=1$, in the model with $U=1$, $D=3$ and the thickness of the buffer layer $L-D=1$. For comparison, the dashed curve shows a single-humped soliton, found also for $k=1$, in the single-channel counterpart of the Kronig-Penney model.

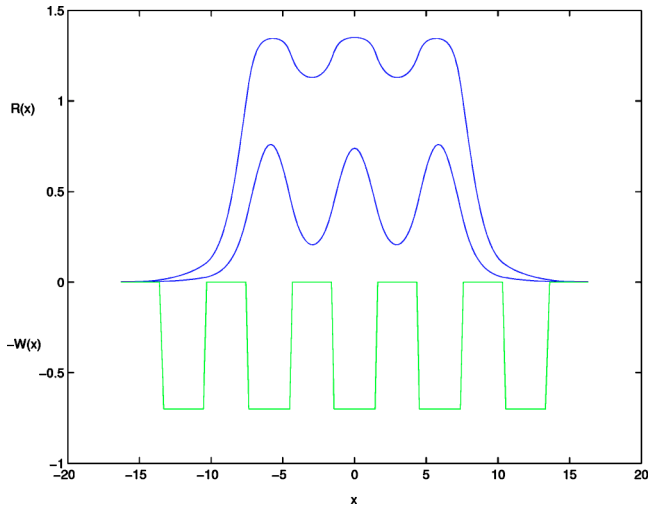

FIG. 13. (Color online) Two three-humped stable solitons, found for $k=1$, in the model with $U=0.7$ and $D=L-D=3$.

two humps with the phase shift of π repel each other, one of the "overpumped" humps makes a jump to an adjacent cell of the KP structure; thus, there appears an antisymmetric soliton with two humps separated by a nearly empty cell (not shown here). In fact, entire families of such double-humped solitons with an empty cell between the peaks can be easily constructed.

IV. THREE-HUMPED AND HIGHER-ORDER SOLITONS

Stationary counterparts of three-humped breathers, such as the one presented in Fig. 3, can be found too, and they all form families. An example of a three-humped (TH) soliton structure with the $(-+-)$ signature of the peaks is shown in Fig. 12. This example stresses that the formation of the TH soliton is specific to the model with the periodic potential, while the CQ model with the single-channel potential supports only SH solitons, with arbitrarily large Q. Examples of the three-humped solitons of the $(+++)$ type are shown in Fig. 13. These examples stress that the three-humped family shares the bistability property with the lower-order solitons.

The dependences $Q(k)$ for the three-humped soliton families are included in Fig. 1. The large gap in the curve for the branch of the $(+++)$ type means that, in the corresponding interval of the values of Q, the numerical procedure could not generate any solution of this type; whether the solutions really do not exist in the gap or merely could not be found remains unclear.

It is instructive to compare the maximum value of the integral power in the latter branch, $Q_{\max}^{(\mathrm{PPPTH})} \approx 27$, to the limit values $Q_{\max}^{(\mathrm{SH})}$ and $Q_{\max}^{(\mathrm{SDH})}$ for the single-humped and symmetric double-humped solitons in the same figure (Fig. 1). Obviously, $Q_{\max}^{(\mathrm{PPPTH})}$ is very close to $3Q_{\max}^{(\mathrm{SH})}$ and, simultaneously, to $(3/2)Q_{\max}^{(\mathrm{DH})}$, which confirms that the TH soliton of the $(+++)$ type is a bound state of three fundamental ones.

V. SOLITONS IN FINITE GAPS IN THE MODEL WITH A STRONG POTENTIAL

While in the case of the weak potential all the solitons exist solely in the semi-infinite band, in the case of a stronger potential, with deeper and/or broader potential wells between the guiding cores, when the KP band structure contains many narrow Bloch bands [see Fig. 6(b)], the solitons are found also in finite gaps between the bands. Typical examples of the corresponding fundamental and double solitons (both symmetric and antisymmetric ones) are displayed in Fig. 14. A drastic difference from the solitons that were found, for a weaker potential, in the semi-infinite gap (cf. Figs. 4 and 7) is the "flat-top" shape of the solitons in the finite gaps (however, they are not absolutely flat inside the waveguiding cores, as it is easy to prove that soliton solutions cannot include constant parts).

An example of the $Q(k)$ characteristic for the full family of the fundamental solitons found in the deep KP potential is shown in Fig. 15 (cf. Fig. 1 for the solitons found in the shallow KP potential, when all solitons belong to the semi-infinite gap). For values of the parameters corresponding to the case shown in Fig. 15, there are five finite Bloch bands (in addition to the semi-infinite one, $k<0$), see Table I. Note that the bands become extremely narrow, obeying the analytical estimate (12).

As is seen in Fig. 15, the gap $0<k<1.002\,96$, which separates the semi-infinite band ($k<0$) and the first finite one, remains empty, while the fundamental-soliton solutions fill the gap between the first and second finite bands. The curve representing the soliton family is cut by the four narrow Bloch bands, and then continues into the semi-infinite gap, where it ends. Families of the symmetric and antisymmetric double solitons have approximately the same structure.

Note that Fig. 15 features no bistability. In fact, detailed examination of the evolution of the $Q(k)$ curves with the increase of the depth U of the KP potential (8) shows that the lower end of the bistable curves (see Fig. 1) moves to the

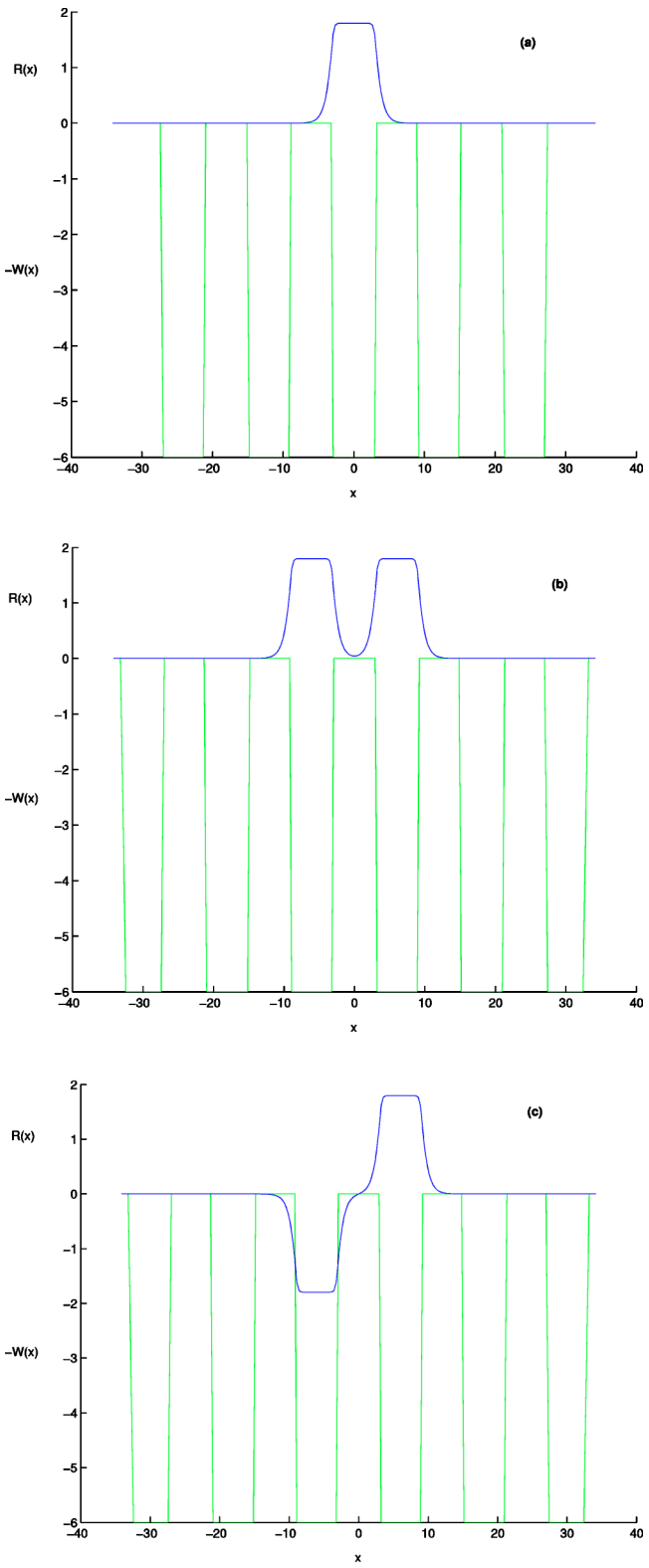

FIG. 14. (Color online) Typical examples of the fundamental (a), double-symmetric (b), and double-antisymmetric (c) solitons with the flat-top shape, found in a finite gap of a deep Kronig-Penney potential, with $U=6$, $D=L-D=6$, and $k=2$. All these solitons are stable.

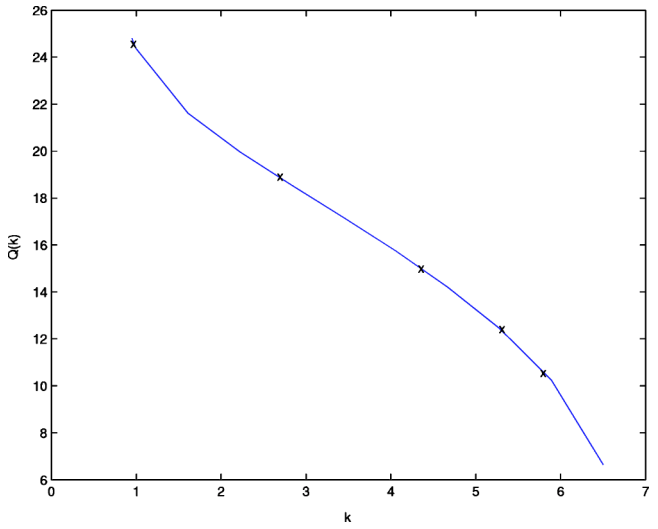

FIG. 15. The curve $Q(k)$ for the family of the fundamental flat-top solitons extending across the finite gaps into the semi-infinite one for $U=6$ and $D=L-D=6$. Crosses show where the curve is cut by very narrow Bloch bands. The exact locations and widths of the bands are given in Table I.

right, approaching the turning point, and, at some critical value of U, the turning point disappears. (Hence, the bistability disappears too.)

Direct simulations demonstrate that all the solitons we have found in the finite gaps are *stable*. An example of stable relaxation of a perturbed fundamental soliton is shown in Fig. 16. Note that the $Q(k)$ curve of the fundamental soliton family in Fig. 15 has a negative slope and thus contravenes the VK criterion (recall the criterion demands $dQ/dk>0$), but the family is, nevertheless, completely stable.

VI. CONCLUSION

We have presented a model combining the Kronig-Penney (KP) potential, in the form of a periodic array of rectangular potential wells, and the cubic-quintic (CQ) nonlinearity. The system supports a plethora of soliton states, including fundamental single-humped solitons, symmetric and antisymmetric double-humped ones, three-peak solitons with and without the phase shift π between the peaks, etc.

TABLE I. Finite Bloch bands in the Kronig-Penney potential (8) with $U=6$ and $D=L-D=6$, the same case as shown in Fig. 15. Each band is found in the corresponding interval $k_{\text{left}}<k<k_{\text{right}}$, with the width $\Delta k=k_{\text{right}}-k_{\text{left}}$. The analytical estimate for the width, $(\Delta k)_{\text{est}}$, is given by Eq. (12).

k_{left}	k_{right}	Δk	$(\Delta k)_{\text{est}}$
1.00296	1.00704	5×10^{-3}	2.5×10^{-3}
2.70203	2.70213	10^{-4}	0.5×10^{-4}
4.116149	4.116156	7×10^{-6}	5×10^{-6}
5.1554377	5.1554386	0.9×10^{-6}	1.2×10^{-6}
5.7878931	5.7878932	10^{-7}	5×10^{-7}

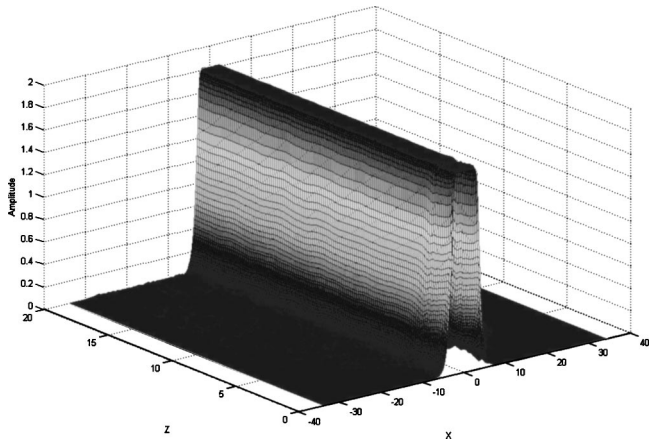

FIG. 16. Stable evolution of a perturbed fundamental soliton belonging to a finite gap whose unperturbed shape is shown in Fig. 14(a).

If the potential is weak, then all the solitons fall into the semi-infinite gap beneath the linear band structure of the KP potential, while finite gaps between the Bloch bands remain empty. However, in contrast with what was found in the model combining a weak periodic potential and the self-focusing Kerr nonlinearity, in the CQ model only a finite zone near the top of the semi-infinite gap is filled by the solitons, which is a consequence of the saturable character of the nonlinearity. In the case when the KP potential is deeper, and/or the buffer layers between the guiding cores are broader, fundamental and double (symmetric and antisymmetric) stable solitons, with a characteristic flat-top shape, are found in finite gaps that separate the Bloch bands in the linear KP model.

Both the computation of stability eigenvalues and direct simulations of perturbed solitons show that they all are stable. As well as in the recently studied CQ model with the single-channel potential, and on the contrary to the model with the Kerr nonlinearity, the soliton families feature bistability, in the form of two (sometimes, even four) different states found for a given propagation constant k, with different values of the integral power Q. However, the bistability disappears in the case of a very deep potential. It is noteworthy that the solution branches with both $dQ/dk>0$ and $dQ/dk<0$ are *stable*, disobeying the Vakhitov-Kolokolov criterion,

Another distinctive feature of the model is the *beam-splitting* property: increase of Q results in a consecutive increase of the number of peaks in the soliton's shape, each corresponding to a subbeam trapped in an individual channel of the periodic structure. This property is explained by an upper bound on the soliton's amplitude in the CQ model, which allows one to increase the beam's power only through its broadening. The broadening leads to the formation of additional peaks in the soliton through trapping of new subbeams in adjacent troughs of the potential structure. The beam splitting and strong stability of the resultant multipeak solitons are effects of direct interest to applications. It is plausible that characteristic features demonstrated by the present model will be shared by more general ones combining a saturable nonlinearity and a periodic potential substrate.

ACKNOWLEDGMENT

This work was supported, in a part, by the Israel Science Foundation through the Grant No. 8006/03.

[1] B. A. Malomed, Z. H. Wang, P. L. Chu, and G. D. Peng, J. Opt. Soc. Am. B **16**, 1197 (1999).
[2] G. L. Alfimov, V. V. Konotop, and M. Salerno, Europhys. Lett. **58**, 7 (2002).
[3] G. L. Alfimov, P. G. Kevrekidis, V. V. Konotop, and M. Salerno, Phys. Rev. E **66**, 046608 (2002).
[4] N. K. Efremidis and D. N. Christodoulides, Phys. Rev. A **67**, 063608 (2003); A. Smerzi and A. Trombettoni, Chaos **13**, 766 (2003).
[5] B. B. Baizakov, B. A. Malomed, and M. Salerno, Europhys. Lett. **63**, 642 (2003).
[6] P. Xie, Z.-Q. Zhang, and X. Zhang, Phys. Rev. E **67**, 026607 (2003); A. Ferrando, M. Zacares, P. F. de Cordoba, D. Binosi, and J. A. Monsoriu, Opt. Express **11**, 452 (2003).
[7] J. W. Fleischer, M. Segev, N. K. Efremidis, and D. N. Christodoulides, Nature (London) **422**, 147 (2003).
[8] B. L. Lawrence, M. Cha, J. U. Kang, W. Torruellas, G. Stegeman, G. Baker, J. Meth, and S. Etemad, Electron. Lett. **30**, 889 (1994); E. W. Wright, B. L. Lawrence, W. Torruellas, and G. I. Stegeman, Opt. Lett. **20**, 2481 (1995); B. L. Lawrence and G. I. Stegeman, *ibid.* **23**, 591 (1998).
[9] F. Smektala, C. Quemard, V. Couderc, and A. Barthélémy, J. Non-Cryst. Solids **274**, 232 (2000); K. Ogusu, J. Yamasaki, S. Maeda, M. Kitao, and M. Minakata, Opt. Lett. **29**, 265 (2004).
[10] C. Zhan, D. Zhang, D. Zhu, D. Wang, Y. Li, D. Li, Z. Lu, L. Zhao, and Y. Nie, J. Opt. Soc. Am. B **19**, 369 (2002).
[11] G. Boudebs, S. Cherukulappurath, H. Leblond, J. Troles, F. Smektala, and F. Sanchez, Opt. Commun. **219**, 427 (2003); F. Sanchez, G. Boudebs, S. Cherukulappurath, H. Leblond, J. Troles, and F. Smektala, J. Nonlinear Opt. Phys. Mater. **13**, 7 (2004).
[12] Y.-F. Chen, K. Beckwitt, F. W. Wise, and B. A. Malomed, Phys. Rev. E **70**, 046610 (2004).
[13] S. Maneuf and F. Reynaud, Opt. Commun. **65**, 325 (1988); J. S. Aitchison, A. M. Weiner, Y. Silberberg, M. K. Oliver, J. L. Jackel, D. E. Leaird, E. M. Vogel, and P. W. E. Smith, Opt. Lett. **15**, 471 (1990).
[14] A. Gammal, T. Frederico, L. Tomio, and P. Chomaz, Phys. Rev. A **61**, 051602 (2000); V. S. Filho, F. K. Abdullaev, A. Gammal, and L. Tomio, *ibid.* **63**, 053603 (2001); F. K. Abdullaev, A. Gammal, L. Tomio, and T. Frederico, *ibid.* **63**, 043604 (2001).
[15] L. Tomio, V. S. Filho, A. Gammal, and T. Frederico, Nucl. Phys. A **684**, 681C (2001).

[16] B. V. Gisin, R. Driben, and B. A. Malomed, J. Opt. B: Quantum Semiclassical Opt. **6**, S259 (2004).
[17] Kh. I. Pushkarov, D. I. Pushkarov, and I. V. Tomov, Opt. Quantum Electron. **11**, 471 (1979); S. Cowan, R. H. Enns, S. S. Rangnekar, and S. S. Sanghera, Can. J. Phys. **64**, 311 (1986).
[18] B. V. Gisin and A. A. Hardy, Phys. Rev. A **48**, 3466 (1993).
[19] N. G. Vakhitov and A. A. Kolokolov, Izv. Vyssh. Uchebn. Zaved., Radiofiz. **16**, 10120 (1973) [in Russian; English translation: Radiophys. Quantum Electron. **16**, 783 (1973)].
[20] B. A. Malomed and R. S. Tasgal, Phys. Rev. E **49**, 5787 (1994); I. V. Barashenkov, D. E. Pelinovsky, and E. V. Zemlyanaya, Phys. Rev. Lett. **80**, 5117 (1998).
[21] R. de L. Kronig and W. G. Penney, Proc. R. Soc. London, Ser. A **130**, 499 (1931); C. Kittel, *Introduction to Solid State Physics* (Wiley, New York, 1995).
[22] W. Li and A. Smerzi, Phys. Rev. E **70**, 016605 (2004).
[23] B. B. Baizakov, V. V. Konotop, and M. Salerno, J. Phys. B **35**, 5105 (2002); V. V. Konotop and M. Salerno, Phys. Rev. A **65**, 021602 (2002); K. M. Hilligsoe, M. K. Oberthaler, and K. P. Marzlin, *ibid.* **66**, 063605 (2002); P. J. Y. Louis, E. A. Ostrovskaya, C. M. Savage, and Y. S. Kivshar, *ibid.* **67**, 013602 (2003).
[24] H. Sakaguchi and B. A. Malomed, J. Phys. B **37**, 1443 (2004).
[25] B. Eiermann, Th. Anker, M. Albiez, M. Taglieber, P. Treutlein, K.-P. Marzlin, and M. K. Oberthaler, Phys. Rev. Lett. **92**, 230401 (2004).